From Hydrogenases to Noble Metal-Free Catalytic Nanomaterials for H_2 Production and Uptake

Le Goff Alan, Artero Vincent, Bruno Jousselme, Dinh Tran Phong, Guillet Nicolas, Romain Metayé, Fihri Aziz, Serge Palacin, Marc Fontecave

constants with V_{vdW}, but are fitted to reproduce the values of $E_{int} + \sigma$ and $E_{int} - \sigma$, respectively, instead of the ab initio interaction energies E_{int}. Both V_+ and V_- support the $v = 11$ state, which lies at respective frequencies 0.38 and 0.70 cm^{-1} below the onset of the continuum. Because the minimum depth of V_+ is 922.1 cm^{-1} (i.e., 8 cm^{-1} shallower than the empirical potential), the well depth is clearly not a determining factor in the appearance of the $v = 11$ state.

The ab initio potential reproduces measured transitions with errors about six times larger than the empirical potential of (*1*). To find out if a closer recovery of the transitions does not lead to disappearance of the $v = 11$ level, we developed a semi-empirical, "morphed" form of V_{vdW}. In the morphing process, the ab initio potential is fine-tuned by introducing a small number (up to five in this work) of adjustable parameters with values fitted to experimental data. The simplest form of morphing is a variation of the energy and length scales in the potential

$$\tilde{V}^{(2)}_{vdW}(R) = aV_{vdW}(bR) \quad (3)$$

via two fitted scaling factors *a*,*b*. The second approach (*8*), an extended version (*13*, *14*) of the reduced potential curve (RPC) method proposed by Jenč and Plíva (*15*), can be viewed as a more general form of scaling. The experimental data points used in the morphing procedure were the vibrational energies and rotational transitions. The fit and the RPC morphing parameters are given in tables S1 and S2.

The predictions of our three morphed potentials are compared with experimental values in Table 1. All show better agreement with measured data than the empirical potential obtained by Merritt *et al*. (*1*). Moreover, there is an order of magnitude improvement relative to the predictions of our ab initio potential, which was distorted to an only minor extent by the morphing (shown by the values of D_e and R_e). All morphed potentials predict the existence of the $v = 11$ level at a position 0.41 to 0.44 cm^{-1} below the dissociation limit, in good agreement with the purely ab initio value. The $v = 11$ vibrational state is not only bound, but supports two excited rotational states.

The failure of the fit of Merritt *et al*. (*1*) to predict the $v = 11$ state can be attributed mainly to its poor asymptotic behavior. Our ab initio calculations were performed for R up to 8 Å, and we used nearly exact van der Waals constants in our fit. Thus, the long-R portion of our fit is very accurate. Merritt *et al*. used a purely exponential form of the fit, which has an unphysical decay at large R. Indeed, the discrepancies of this fit relative to V_{vdW} are up to 2.4 cm^{-1} in the 5 to 8 Å range where the interaction potential ranges between −87 and −5 cm^{-1}. This region is critical for the high-v states, as shown in Fig. 1. The vibrational wave function of the $v = 11$ state has a maximum magnitude around 10 Å. Because this wave function is mainly sensitive to the region of the potential well approximated by the asymptotic $-C_6/R^6$ term, one can use the semi-classical near-dissociation theory of Le Roy and Bernstein (*16*) to determine the number of bound levels. If the experimental dissociation energies of the $v = 9$ and $v = 10$ states are used as input, this theory predicts that there exists one more bound vibrational state above these two. It is gratifying to see that the simple qualitative picture of the near-dissociation theory agrees with our quantitative ab initio description of vibrational levels in the beryllium dimer.

References and Notes

1. J. M. Merritt, V. E. Bondybey, M. C. Heaven, *Science* **324**, 1548 (2009).
2. V. E. Bondybey, *Chem. Phys. Lett.* **109**, 436 (1984).
3. V. E. Bondybey, *Science* **227**, 125 (1985).
4. P. Blythe, B. Roth, U. Frohlich, H. Wenz, S. Schiller, *Phys. Rev. Lett.* **95**, 183002 (2005).
5. I. Røeggen, J. Almlöf, *Int. J. Quantum Chem.* **60**, 453 (1996).
6. K. Patkowski, R. Podeszwa, K. Szalewicz, *J. Phys. Chem. A* **111**, 12822 (2007).
7. K. T. Tang, J. P. Toennies, *J. Chem. Phys.* **80**, 3726 (1984).
8. Materials and methods are available as supporting material on *Science* Online.
9. J. M. L. Martin, *Chem. Phys. Lett.* **303**, 399 (1999).
10. R. J. Gdanitz, *Chem. Phys. Lett.* **312**, 578 (1999).
11. I. Røeggen, L. Veseth, *Int. J. Quantum Chem.* **101**, 201 (2005).
12. V. Špirko, *J. Mol. Spectrosc.* **235**, 268 (2006).
13. O. Bludský, M. Juřek, V. Špirko, B. A. Brandt, F. Jenč, *J. Mol. Spectrosc.* **169**, 555 (1995).
14. V. Špirko, *Collect. Czech. Chem. Commun.* **70**, 731 (2005).
15. F. Jenč, J. Pliva, *Collect. Czech. Chem. Commun.* **19**, 1449 (1962).
16. R. J. Le Roy, R. B. Bernstein, *Chem. Phys. Lett.* **5**, 42 (1970).

17. This work was supported by the NSF grant CHE-0848589, by the Academy of Sciences of the Czech Republic grant IAA400550511 (project Z40550506), and by the Czech Ministry of Education, Youth and Sports grants LC512 and MSM6198959216.

Supporting Online Material

www.sciencemag.org/cgi/content/full/326/5958/1382/DC1
SOM Text
Fig. S1
Tables S1 and S2
References

24 August 2009; accepted 14 October 2009
10.1126/science.1181017

From Hydrogenases to Noble Metal–Free Catalytic Nanomaterials for H_2 Production and Uptake

Alan Le Goff,[1] Vincent Artero,[2]* Bruno Jousselme,[1] Phong Dinh Tran,[2] Nicolas Guillet,[3] Romain Métayé,[1] Aziz Fihri,[2] Serge Palacin,[1]* Marc Fontecave[2,4]

Interconversion of water and hydrogen in unitized regenerative fuel cells is a promising energy storage framework for smoothing out the temporal fluctuations of solar and wind power. However, replacement of presently available platinum catalysts by lower-cost and more abundant materials is a requisite for this technology to become economically viable. Here, we show that the covalent attachment of a nickel bisdiphosphine–based mimic of the active site of hydrogenase enzymes onto multiwalled carbon nanotubes results in a high–surface area cathode material with high catalytic activity under the strongly acidic conditions required in proton exchange membrane technology. Hydrogen evolves from aqueous sulfuric acid solution with very low overvoltages (20 millivolts), and the catalyst exhibits exceptional stability (more than 100,000 turnovers). The same catalyst is also very efficient for hydrogen oxidation in this environment, exhibiting current densities similar to those observed for hydrogenase-based materials.

One dilemma inherent in the widespread use of solar cells and windmills for power generation is that temporal fluctuations in worldwide energy demand do not strictly correlate with the availability of sunlight and wind. An efficient, reversible means of storing excess energy is necessary, and unitized regenerative fuel cells are an attractive option for that purpose. The devices operate by storing energy in hydrogen generated via electrolysis of water and then releasing it as necessary through the reverse reaction. The devices are compact and have low internal resistance. However, they currently rely on platinum for catalysis, which is too scarce and thus too expensive for widespread adoption (*1*). A competitive alternative may be found in microorganisms that metabolize hydrogen using hydrogenase enzymes (*2*, *3*). These metalloproteins bidirectionally catalyze interconversion between H_2 and a pair of protons and electrons (the same

[1]Commissariat à l'Énergie Atomique (CEA), Institut Rayonnement Matière de Saclay, Service de Physique et Chimie des Surfaces et Interfaces, Chemistry of Surfaces and Interfaces group, F-91191 Gif sur Yvette Cedex, France. [2]Laboratoire de Chimie et Biologie des Métaux, Université Joseph Fourier, CNRS UMR 5249, CEA Institut de Recherche en Technologies et Sciences pour le Vivant, 17 rue des Martyrs, F-38054 Grenoble cedex 9, France. [3]Institut Laboratoire d'Innovation pour les Technologies des Energies Nouvelles et les Nanomatériaux (LITEN), CEA LITEN/Département des Technologies de l'Hydrogène, Laboratoire des composants pour Pile à combustible, Electrolyse et Modélisation, 17 rue des Martyrs, F-38054 Grenoble cedex 9, France. [4]Collège de France, 11 place Marcellin-Berthelot, F-75005 Paris, France.

*To whom correspondence should be addressed. E-mail: vincent.artero@cea.fr (V.A.); serge.palacin@cea.fr (S.P.)

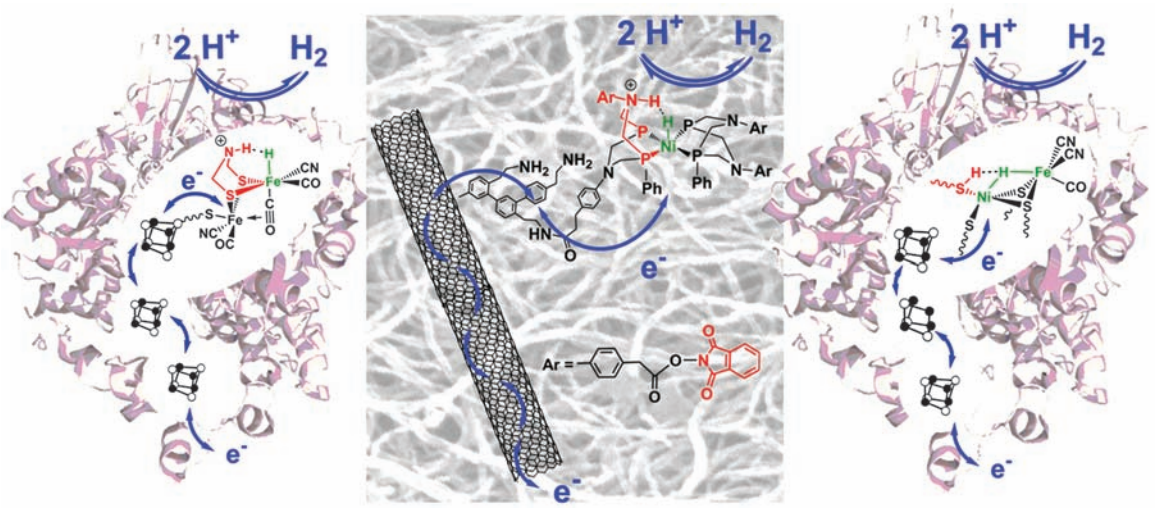

Fig. 1. Architectures of FeFe (**Left**) and NiFe (**Right**) hydrogenases in the reduced active state and schematic representation of the structure of the bio-inspired H_2-evolving nickel catalyst grafted on a carbon nanotube (**Middle**). The structure of the activated phtalimide ester moieties introduced in para position of the nitrogen-bound phenyl residues of the diphosphine ligands in $\mathbf{2}(BF_4)_2$ is also indicated. Blue arrows trace the electron transport chain toward the active site, either through iron-sulfur clusters in the enzymes or through the conductive CNT. The ligands acting as proton relays in heterolytic hydrogen evolution reaction are depicted in red, and the metal centers stabilizing hydride ions are depicted in green. In this simplified representation, the number of phenylene residues shown is arbitrary, and we do not exclude attachment of the nickel complex to two or more surface amine groups.

reaction taking place at electrodes in fuel cells and electrolyzers) as efficiently as platinum nanoparticles do and with remarkably high reaction rates (1500 to 9000 s^{-1} at pH 7 and 37°C in water) (*4*). In addition, when adsorbed on an electrode they operate without the need for any additional applied voltage beyond the equilibrium potential for the H_2O/H_2 couple (*5*–*7*). Unfortunately, hydrogenases suffer from considerable oxygen sensitivity. In addition, their production in the active form can hardly be scaled up to satisfy technological demand.

Because catalysis in hydrogenases requires only iron and nickel metal centers, the active sites (Fig. 1) are strong sources of inspiration for the design of synthetic catalysts that are more sustainable than platinum (*6*, *8*–*13*). In addition, bio-inspired synthetic catalysts are easy to prepare and can often be handled in air, which is key for the integration in a technological device. One of the most successful achievements of the biomimetic approach involves a family of bisdiphosphine nickel complexes (*11*, *14*) that combine very well a nickel center in an electron-rich environment (as found in NiFe hydrogenases) with proton relays provided by a pendant base mimicking the putative azapropanedithiolato cofactor of FeFe hydrogenases (*15*). The presence of basic residues at the vicinity of the catalytic metal center indeed facilitates the formation of H_2 from a coordinated hydride ion and a proton from the ammonium group (Fig. 1). It is thus tempting to address the issue of whether such biomimetic molecular systems can be exploited for the development of efficient and robust electrode materials.

To this end, we have explored the prospect of assembling an electrode by binding these biomimetic nickel complexes to carbon nanotubes (CNTs). Among the advantages of CNTs for this purpose are their high surface areas (facilitating high catalyst loading), their high stability and electrical conductivity (*16*, *17*), and the availability of versatile and straightforward methods

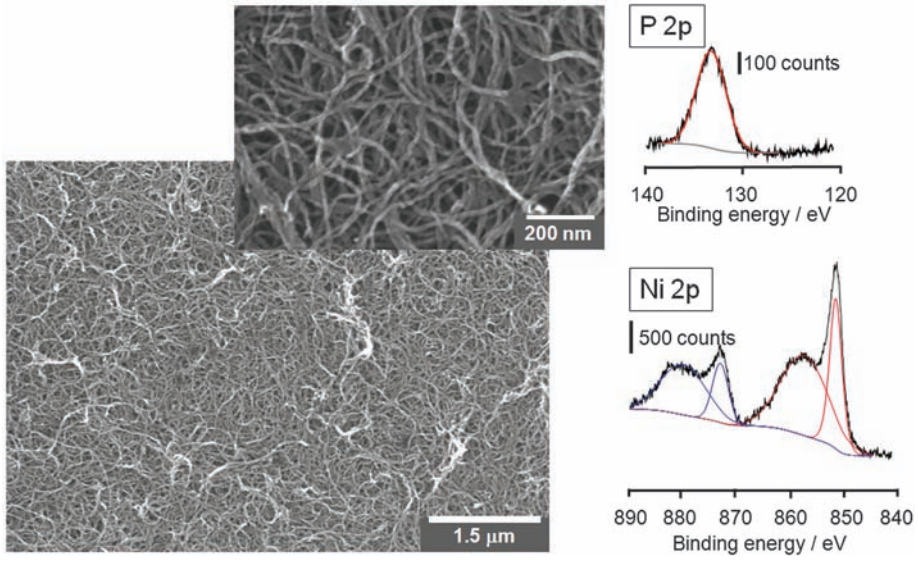

Fig. 2. Scanning electron micrographs of a ITO/MWCNT electrode and decomposed x-ray photoelectron spectra of a Ni-functionalized ITO/MWCNT electrode at (**Top**) P 2p and (**Bottom**) Ni 2p energy levels (red, $2p_{3/2}$; blue, $2p_{1/2}$).

for grafting molecular complexes onto their surfaces (*18*–*20*). For example, electro-reduction of functionalized aryldiazonium salts has been recently used to modify CNT-based electrodes by means of hydrogenases that yield highly active electrocatalytic materials, although these electrodes are useable only under inert atmosphere (*21*).

Cyclic voltammetry (CV) showed that electrodes prepared by depositing a thin film of multiwall CNTs (MWCNTs) (*22*) onto an indium tin oxide (ITO) substrate (fig. S1) by means of a soluble membrane technique reported by Wu *et al.* (*23*) display a quasi-reversible response for ferrocene oxidation in CH_3CN with a peak-to-peak separation (ΔE) of 90 mV (*24*). The high electrode surface area was shown by means of scanning electron microscopy (SEM) (Fig. 2), which revealed bundles of MWCNTs with extensive branching. Covalent attachment of 4-(2-aminoethyl)phenyl groups at the surface of these electrodes was optimally achieved via the electro-reduction of the corresponding protonated diazonium tetrafluoroborate salt $\mathbf{1}(BF_4)_2$ (*25*), cycling between 0.8 and 0.0 V versus normal hydrogen electrode (NHE) at 20 mV s^{-1}. The first scan indicated an irreversible cathodic process ($E_p^c = 0.22$ V versus NHE) corresponding to the grafting of a polyphenylene layer on the MWCNTs electrode (fig. S2). On the two successive scans, a deviation of the reduction peak toward more negative potentials was observed, which is indicative of continuous growth of a conductive polyphenylene layer (Fig. 1). Three-scan CV affords the most homogeneous coverage and the maximum number of

available amine sites (*26*). X-ray photoelectron spectroscopy (XPS) analysis confirmed the presence of both amine and ammonium groups with respective peaks at 399.9 and 401.6 eV corresponding to the energies of the 1 s orbital on the N atom (fig. S3).

Activated phtalimide ester moieties (Fig. 1) have been introduced in para position of the nitrogen-bound phenyl residues of the 1,3,5,7-tetraphenyl-1,5-diaza-3,7-diphosphacyclooctane ligand initially reported by Wilson *et al.* (*14*). The resulting hydrogenase-inspired nickel catalyst **2**$(BF_4)_2$ is air- and moisture-stable, thus straightforward to anchor to the amino-functionalized MWCNT-electrode material via the formation of stable covalent amide linkages. The cyclic voltammogram of **2**$(BF_4)_2$ displays two quasi-reversible cathodic processes at –0.34V (ΔE = 170 mV) and –0.53V versus NHE (ΔE = 100 mV) in CH_3CN (fig. S4 and table S1) (*27*). Addition of a triflate (OTf) salt of protonated dimethylformamide (DMF) [[DMFH]OTf/DMF 1:1 mol/mol, pK_a = 6.1 in CH_3CN (where K_a is the acid dissociation constant), $E°([DMFH]^+/H_2)$ = –0.08 V versus NHE] as an acid source triggers the appearance of an electrocatalytic wave at $E_{1/2}$ = –0.30 V versus NHE assigned to hydrogen evolution (fig. S5). This electrocatalytic behavior is similar to that of the parent complex containing the unfunctionalized 1,3,5,7-tetraphenyl-1,5-diaza-3,7-diphosphacyclooctane ligand (*11*) with respect to redox potential as well as catalytic current enhancement, expressed as the i_c/i_p ratio [where i_c is the catalytic current and i_p is the peak current associated with the $Ni^{II/I}$ couple]. This ratio varies linearly with acid concentration and reaches a plateau at i_c/i_p = 5 and [$DMFH^+$] = 5 mM (fig. S6). The parent complex behaved similarly but plateaued at [$DMFH^+$] = 300 mM and i_c/i_p = 50 (*11*). This difference might arise from the presence of the four bulky anchor groups in **2**$(BF_4)_2$, which slow down the conformational changes required during the catalytic cycle so as to position the proton relays in the vicinity of the metal active site.

Compound **2**$(BF_4)_2$ was successfully anchored to the amino-functionalized electrode in room-temperature CH_3CN through the formation, in the presence of Et_3N, of amide linkages between the ligand of **2**$(BF_4)_2$ and the grafted amine residues. A schematic representation of the resulting functionalized CNTs film is displayed in Fig. 1. The material was characterized by means of CV in CH_3CN and XPS. The cyclic voltammogram (black trace in Fig. 3A) displays a cathodic process at –0.59 V versus NHE (ΔE = 120 mV) assigned to the reduction of the grafted Ni^{II} complex. This signal probably corresponds to a combination of the two monoelectronic waves formerly observed in solution. We posit that these features merge because the first electron transfer step has been slowed, and the corresponding potential shifted to a more negative value, upon complex grafting as a result of an increased reorganization energy of the nickel coordination sphere (*28*). Surface catalyst concentration as high as 1.5 (±0.5) × 10^{-9} mol cm^{-2} could be estimated from the integration of this wave. For comparison, rough ITO electrodes directly functionalized with **2**$(BF_4)_2$ through the reduction of the diazonium salt **1**$(BF_4)_2$ by using the same two-step procedure exhibit surface nickel concentrations in the range of 4.5 (±1.5) × 10^{-11} mol cm^{-2}. The high specific surface provided by the film of MWCNTs thus raises catalyst concentration by almost two orders of magnitude. This difference was reflected in the much larger current response observed in the CV of the Ni-functionalized ITO/MWCNT electrode as compared with a Ni-functionalized ITO electrode (fig. S7).

XPS analysis (Fig. 2 and fig. S8) confirms the presence of the intact nickel complex at the surface of the electrode. Analysis of the Ni $2p_{3/2}$ region shows one sharp peak centered at 856.0 eV, which is a signature of the Ni^{II} ion, whereas the P 2p peak centered at 132.2 eV confirms the presence of metal-bound phosphorous atoms.

Protonation of the grafted nickel complex occurs upon addition of [DMFH]OTf/DMF (1:1 mol/mol) and results in the observation of an irreversible reductive process (E_p^c = –0.31 V versus NHE) 280 mV more positive than that exhibited by grafted **2**$(BF_4)_2$ (Fig. 3A). The electrocatalytic nature of this wave is evidenced by the linear increase of the normalized peak current (i_c/i_p) with increased acid concentration (fig. S9). The electrocatalytic properties of the nickel complex are thus retained in the grafted material, and the electroconductive properties of the MWCNTs induce

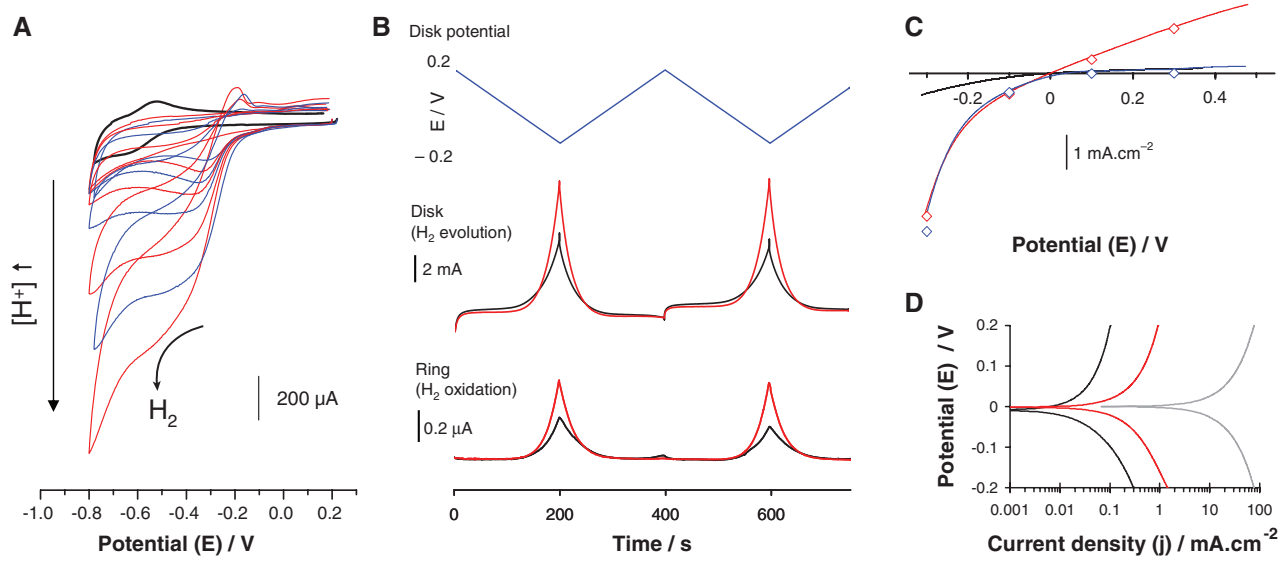

Fig. 3. (**A**) Electrocatalytic behavior of a nickel functionalized ITO/MWCNT electrode (1 cm^2) in CH_3CN with 0.2 M Bu_4NPF_6 electrolyte at various concentrations of the acid 1:1 mol/mol [DMFH]OTf/DMF (0.29, 0.60, 0.90, 1.17, 1.75, 2.34, 3.51, 5.85, and 11.7 mM) (50 mV s^{-1} scan rate). The cyclic voltammogram recorded in the absence of acid is shown in black. (**B**) Rotating ring-disk electrode measurements (5 mV s^{-1}) of hydrogen evolution from a 0.5 M H_2SO_4 aqueous solution on MWCNTs (black) and Ni-functionalized MWCNTs (red) coated with Nafion on a glassy carbon electrode. (Top) Disk potential. (Middle) Disk current density. (Bottom) Pt-ring current (the Pt-ring was held at 0.6 V). (**C**) Evolution of current density as a function of potential for both hydrogen production and uptake from a 0.5 M H_2SO_4 aqueous solution, recorded at a MEA consisting of a GDL assembled with a Nafion membrane (2 mV s^{-1}). Black, unfunctionalized GDL; blue, Ni-functionalized GDL/MWCNT under an atmosphere of N_2; red, Ni-functionalized GDL/MWCNT under an atmosphere of H_2 (10^5 Pa). The *x* axis is positioned at 0 current density. Dots represent stabilized values of current at electrodes set for 10 min at various potentials. (**D**) Logarithmic plots of current density as a function of the potential for both hydrogen production and uptake. The black and red traces correspond to the measurements shown in (C) with the same colors; the gray trace is a measurement on a commercial MEA containing highly dispersed platinum (0.5 mg_{Pt} cm^{-2}). Similar logarithmic plots are obtained when Ni-functionalized MWCNTs are deposited on a glassy carbon disk electrode. Potentials are quoted versus NHE.

a remarkably low overvoltage (200 mV) for hydrogen evolution. For comparison, pristine MWCNTs mediate hydrogen evolution from the same medium at –0.7 V versus NHE (fig. S10), corresponding to a much larger overvoltage (600 mV).

The material's stability and associated ability to catalyze sustained production of H_2 was investigated by means of controlled-potential coulometry experiments in nonaqueous media. The electrolysis of a CH_3CN solution of [DMFH]OTf/DMF (1:1 mol/mol, 0.1 mol.L^{-1}) was performed at a potential of –0.5 V versus NHE in an electrochemical cell coupled to a U-tube for volumetric analysis and a gas chromatograph equipped with a catharometer for hydrogen detection. Under these conditions, H_2 is produced with a sustained current density (J) of 2 mA cm^{-2}. XPS analysis performed after a 1-hour electrolysis experiment confirmed the presence of a molecular nickel-phosphine complex. A >94% faradaic yield can be estimated from the charge (3 C) passed through the electrode (0.5 cm^2) and the amount of hydrogen (15 mmol) produced within 1 hour. Using the surface concentration of the catalyst estimated earlier [1.5 (± 0.5) × 10^{-9} mol.cm^{-2}] affords a turnover number of 20,000 (±30%) achieved within 1 hour. For comparison, previously reported stable molecular catalytic materials based on cobalt porphyrins (*29*) or organometallic rhodium complexes (*30*), incorporated in a Nafion membrane or polypyrrole film, show overvoltages greater than 400 mV or turnover frequencies limited to a few tenths per hour.

Practical applications of such molecular electrode materials require the use of aqueous electrolytes. Catalytic hydrogen production from diluted (pH of 0 to 1) sulfuric acid solutions was demonstrated in two ways. First, we dropcoated an ink made of Ni-functionalized MWCNTs (50 μg) dispersed in a 5 weight percent solution [Nafion dispersion type D520 (DuPont, Wilmington, Delaware)] onto a glassy carbon-disc electrode. After drying, rotating electrode measurements (Fig. 3B) confirmed that H_2 can be produced on the disc electrode and simultaneously detected at a concentric platinum ring held at 0.6 V versus NHE. Analysis of the voltammograms revealed that electrocatalytic hydrogen evolution occurred with an overvoltage of 20 mV, less than a sixth of that observed on pristine MWCNTs (128 mV). Second, we assayed our material in a half-cell configuration, reproducing the experimental conditions found in state-of-the-art proton exchange membrane (PEM) electrolyzers but with the platinum-based active layer replaced by Ni-functionalized MWCNTs. A membrane-electrode assembly (MEA) prepared for that purpose consisted of a Nafion membrane hot-pressed with a gas diffusion layer (GDL), on which the MWCNTs were deposited and further functionalized with **2**$(BF_4)_2$. This MEA displayed an electrocatalytic activity for hydrogen evolution much higher than that of unfunctionalized GDL or pristine MWCNTs deposited on GDL under similar conditions (Fig. 3C). A current density of about 4 mA cm^{-2} was measured at 300 mV overvoltage. The stabilized current values measured at a MEA after holding for 10 min at various potentials matched those of the initial voltammogram. This evidence of catalyst stability precludes the formation of nickel-based particles as the catalytically active species. In any case, from the Pourbaix diagram, either nickel oxide/hydroxide compounds or elemental nickel would be unstable under the assay conditions. This MEA was held at –300 mV versus NHE in 0.5 M H_2SO_4 for 10 hours. The current density keeps constant throughout the experiment, with more than 100,000 (±30%) turnovers achieved (fig. S12). Hydrogen evolution was monitored by using gas chromatography during the first 30 min and was found to occur with a quantitative faradaic yield.

The unexpectedly low overvoltage observed here for hydrogen production prompted us to explore this material as a catalyst for the reverse reaction, catalytic hydrogen oxidation. The same membrane-electrode assembly was assayed under the same conditions as described above, except that a hydrogen atmosphere was used instead of nitrogen. In the corresponding voltammogram (Fig. 3C), the cathodic response—hydrogen production—is almost unchanged. However, the anodic wave indicates hydrogen oxidation with a current density of about 2 mA cm^{-2} at 500 mV overvoltage, similar to that found for hydrogenase-modified carbon material such as carbon felt (*31*) or MWCNT electrodes (*21*). The catalytic current, recorded at a lower overvoltage (300 mV), is stable during a 10-hour electrolysis experiment, corresponding to 35,000 (±30%) turnovers (fig. S12). The shape of the voltammogram for positive potentials indicates a kinetic limitation due to the diffusion of hydrogen at the grafted active sites. The same effect has been observed for immobilized hydrogenases (*5*). A logarithmic plot of the current density as a function of potential (Fig. 3D) highlights the transition between H_2 oxidation and production. The point of 0 current density nearly overlaps the standard potential of the H^+/H_2 couple under the experimental conditions, thus confirming the low overvoltage of our Ni-functionalized MEA for H^+/H_2 interconversion. Figure 3D also compares our MEA with a commercial MEA containing highly dispersed platinum (0.5 mg Pt cm^{-2}), which exhibits a current density about two orders of magnitude higher than that of the Ni/MWCNT system. This performance discrepancy is nonetheless balanced by the fact that the latter catalyst loading is limited to 0.06 mg cm^{-2} of an earth-abundant metal. Our results show that the biomimetic nanomaterial reported here offers promising turnover rates under conditions compatible with widespread PEM technology on the basis of commercial proton exchange membranes in acidic electrolytes.

References and Notes

1. R. Bashyam, P. Zelenay, *Nature* **443**, 63 (2006).
2. A. Volbeda *et al.*, *Nature* **373**, 580 (1995).
3. J. W. Peters, W. N. Lanzilotta, B. J. Lemon, L. C. Seefeldt, *Science* **282**, 1853 (1998).
4. V. Artero, M. Fontecave, *Coord. Chem. Rev.* **249**, 1518 (2005).
5. K. A. Vincent, A. Parkin, F. A. Armstrong, *Chem. Rev.* **107**, 4366 (2007).
6. S. Canaguier, V. Artero, M. Fontecave, *Dalton Trans.* 315 (2008).
7. J. C. Fontecilla-Camps, A. Volbeda, C. Cavazza, Y. Nicolet, *Chem. Rev.* **107**, 5411 (2007).
8. C. Tard *et al.*, *Nature* **433**, 610 (2005).
9. S. Ogo *et al.*, *Science* **316**, 585 (2007).
10. C. Mealli, T. B. Rauchfuss, *Angew. Chem. Int. Ed.* **46**, 8942 (2007).
11. A. D. Wilson *et al.*, *Proc. Natl. Acad. Sci. U.S.A.* **104**, 6951 (2007).
12. Z. L. Li, Y. Ohki, K. Tatsumi, *J. Am. Chem. Soc.* **127**, 8950 (2005).
13. M. L. Singleton, N. Bhuvanesh, J. H. Reibenspies, M. Y. Darensbourg, *Angew. Chem. Int. Ed.* **47**, 9492 (2008).
14. A. D. Wilson *et al.*, *J. Am. Chem. Soc.* **128**, 358 (2006).
15. The exact nature of this basic site at the active site of FeFe hydrogenases has been subject to debate, but recent spectroscopic data are in favor of a nitrogen atom (*32*).
16. D. Tasis, N. Tagmatarchis, A. Bianco, M. Prato, *Chem. Rev.* **106**, 1105 (2006).
17. V. Sgobba, D. M. Guldi, *Chem. Soc. Rev.* **38**, 165 (2009).
18. B. Jousselme *et al.*, *J. Electroanal. Chem.* **621**, 277 (2008).
19. J. Pinson, F. Podvorica, *Chem. Soc. Rev.* **34**, 429 (2005).
20. J. L. Bahr *et al.*, *J. Am. Chem. Soc.* **123**, 6536 (2001).
21. M. A. Alonso-Lomillo *et al.*, *Nano Lett.* **7**, 1603 (2007).
22. We chose MWCNTs for their metallic electron conductivity. In addition, they do not require noble metal catalysts for growth and can be easily obtained in high purity.
23. Z. C. Wu *et al.*, *Science* **305**, 1273 (2004).
24. Materials and methods are available as supporting material on *Science* Online.
25. S. Griveau, D. Mercier, C. Vautrin-Ul, A. Chaussé, *Electrochem. Commun.* **9**, 2768 (2007).
26. Alternatively, electrografting can be achieved at a fixed potential of 0.16 V versus NHE with a total charge of 15 mC passed through a 1 cm^2 electrode.
27. Bulk electrolysis of **2**$(BF_4)_2$ carried out at –0.75 V versus NHE in CH_3CN confirmed an overall two-electron reduction process, with 1.83 electrons per complex passing through the cell within 3 hours.
28. To support this assignment, we performed a control experiment that entailed grafting a ferrocene derivative, possessing the same activated ester function, instead of the nickel complex. The yield of the second step in the functionalization procedure is probably the same for both complexes. In that case, the typical monoelectronic quasi-reversible process is observed in CH_3CN at 420 mV versus NHE. Integration area of the anodic peak is about half of that obtained with the nickel complex.
29. T. Abe *et al.*, *Polym. Adv. Technol.* **9**, 559 (1998).
30. S. Cosnier, A. Deronzier, N. Vlachopoulos, *J. Chem. Soc. Chem. Commun.* 1259 (1989).
31. M. Hambourger *et al.*, *J. Am. Chem. Soc.* **130**, 2015 (2008).
32. A. Silakov, B. Wenk, E. Reijerse, W. Lubitz, *Phys. Chem. Chem. Phys.* **11**, 6592 (2009).

33. This work was supported by the CEA (Nanosciences program, grant Grafthydro), the CNRS ("Materials" program, grant 961 "projets exploratoires: Interface Science des Matériaux/Vivant") and the Agence Nationale de la Recherche (PAN-H 2008, EnzHyd). The authors thank E. Mayousse and P.-A. Jacques for experimental contribution and V. Derycke for assistance in the SEM characterizations. The authors have filed a European patent application (EP-08 290 988.8) for the grafting procedure of catalysts presented here.

Supporting Online Material

www.sciencemag.org/cgi/content/full/326/5958/1384/DC1
Materials and Methods
Figs. S1 to S12
Table S1
References

28 July 2009; accepted 13 October 2009
10.1126/science.1179773

Science

From Hydrogenases to Noble Metal–Free Catalytic Nanomaterials for H_2 Production and Uptake

Alan Le Goff, Vincent Artero, Bruno Jousselme, Phong Dinh Tran, Nicolas Guillet, Romain Métayé, Aziz Fihri, Serge Palacin and Marc Fontecave

Science **326** (5958), 1384-1387.
DOI: 10.1126/science.1179773

Electrolysis at Nickel

One drawback of solar and wind power is the need for an efficient storage system to release accumulated energy when neither source is readily available (during still nights, for example). Hydrogen derived from electrolysis of water is potentially a useful medium for this purpose, but catalyzing the interconversion efficiently at large scale would currently require a substantial amount of the scarce precious metal platinum. An alternative approach would be to mimic natural enzymatic reactions, which accomplish the interconversion using hydrogenases that incorporate the more abundant metals iron and nickel. In this vein, **Le Goff *et al.*** (p. 1384; see the Perspective by **Hambourger and Moore**) have lightly modified a hydrogenase-inspired nickel complex in order to append it to a conductive carbon nanotube support. The resulting hybrid material shows promising catalytic efficiency for reversible aqueous electrolysis in a standard apparatus.

Science (print ISSN 0036-8075; online ISSN 1095-9203) is published by the American Association for the Advancement of Science, 1200 New York Avenue NW, Washington, DC 20005. The title *Science* is a registered trademark of AAAS.